

NRC Publications Archive Archives des publications du CNRC

Hydrokinetic resource assessment for the Canadian Arctic for turbine-based power generation

Bhattacharjee, Koyena; Sushama, Laxmi; Cousineau, Julien

This publication could be one of several versions: author's original, accepted manuscript or the publisher's version. / La version de cette publication peut être l'une des suivantes : la version prépublication de l'auteur, la version acceptée du manuscrit ou la version de l'éditeur.

For the publisher's version, please access the DOI link below. / Pour consulter la version de l'éditeur, utilisez le lien DOI ci-dessous.

Publisher's version / Version de l'éditeur:

<https://doi.org/10.2166/wcc.2025.353>

Journal of Water and Climate Change, 16, 4, pp. 1238-1259, 2025-03-12

NRC Publications Archive Record / Notice des Archives des publications du CNRC :

<https://nrc-publications.canada.ca/eng/view/object/?id=eb984ce0-ca0c-472b-ae52-91e11f8b4e9e>

<https://publications-cnrc.canada.ca/fra/voir/objet/?id=eb984ce0-ca0c-472b-ae52-91e11f8b4e9e>

Access and use of this website and the material on it are subject to the Terms and Conditions set forth at

<https://nrc-publications.canada.ca/eng/copyright>

READ THESE TERMS AND CONDITIONS CAREFULLY BEFORE USING THIS WEBSITE.

L'accès à ce site Web et l'utilisation de son contenu sont assujettis aux conditions présentées dans le site

<https://publications-cnrc.canada.ca/fra/droits>


LISEZ CES CONDITIONS ATTENTIVEMENT AVANT D'UTILISER CE SITE WEB.

Questions? Contact the NRC Publications Archive team at

PublicationsArchive-ArchivesPublications@nrc-cnrc.gc.ca. If you wish to email the authors directly, please see the first page of the publication for their contact information.

Vous avez des questions? Nous pouvons vous aider. Pour communiquer directement avec un auteur, consultez la première page de la revue dans laquelle son article a été publié afin de trouver ses coordonnées. Si vous n'arrivez pas à les repérer, communiquez avec nous à PublicationsArchive-ArchivesPublications@nrc-cnrc.gc.ca.

Hydrokinetic resource assessment for the Canadian Arctic for turbine-based power generation

Koyena Bhattacharjee ^{a,*}, Laxmi Sushama^a and Julien Cousineau^b

^a Department of Civil Engineering, Trottier Institute for Sustainability in Engineering and Design, McGill University, Montreal, QC, Canada

^b The Ocean Coastal and River Engineering Research Center of the National Research Council Canada, Ottawa, ON, Canada

*Corresponding author. E-mail: koyena.bhattacharjee@mail.mcgill.ca

 KB, 0009-0000-9984-0891

ABSTRACT

Renewable energy development has rekindled interest in hydrokinetic power production using zero-head turbines. This study estimates the hydrokinetic power potential for current-based systems in the Canadian Arctic, primarily Nunavut, for the current 2001–2020 and near-future 2021–2040 periods, based on streamflow obtained from an ultra-high-resolution climate-hydrology modeling system for a high emission scenario. A comparison of simulated hydrographs with available observations suggests good agreement, with the Nash Sutcliffe efficiency coefficient in the 0.85–0.96 range. Spatial patterns of hydrokinetic power estimates, which are similar to that of flow velocity, indicate a potential of above 100,000 kW for river reaches in central Nunavut for current/future climates. Investigation of the number of days with flow velocities surpassing the 1.5 m/s threshold for turbine functionality, considering also the impact of river ice using a simplified approach, confirms segments of central basin rivers as promising sites for hydrokinetic turbine placement. This foundational work is crucial in informing detailed site-specific investigations to support the implementation of hydrokinetic energy conversion systems. This will be of interest for remote communities in the Canadian Arctic where decentralized power production from renewable energy sources is being considered as an economically viable option in offsetting the high cost of diesel-based power production.

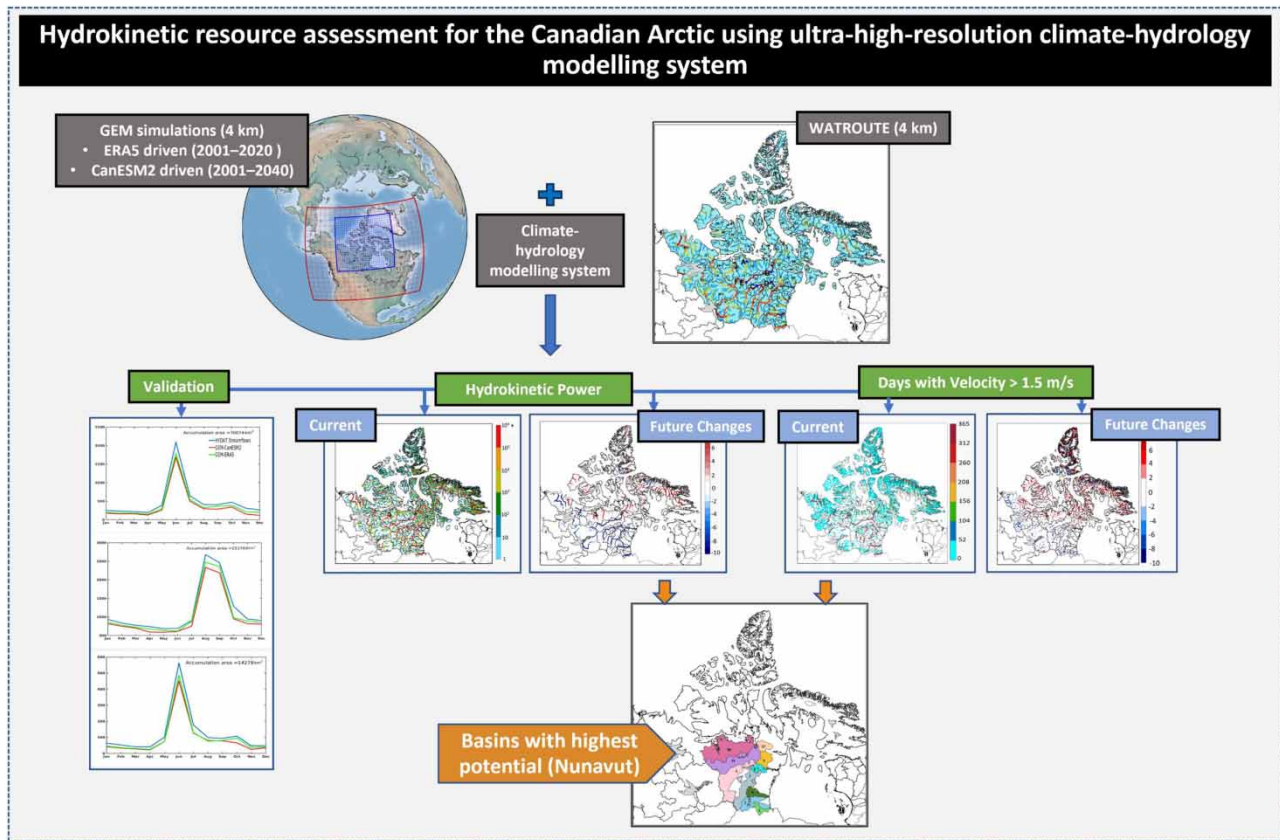
Key words: Canadian Arctic, climate-hydrology integrated modeling, high-resolution regional climate simulations, hydrokinetic power, streamflow

HIGHLIGHTS

- Very first ultra-high-resolution estimates of hydrokinetic power for the high-latitude regions of Canada for current and near-future climates.
- Central basins of Nunavut were identified as potential regions for hydrokinetic power generation.
- Beneficial to remote communities in the Canadian Arctic with its potential to offset the reliance on diesel-based power production.

This is an Open Access article distributed under the terms of the Creative Commons Attribution Licence (CC BY-NC 4.0), which permits copying, adaptation and redistribution for non-commercial purposes, provided the original work is properly cited (<http://creativecommons.org/licenses/by-nc/4.0/>).

GRAPHICAL ABSTRACT



1. INTRODUCTION

With the increasing energy demand (WHO 2009) and the continued warming of the Arctic regions at double the rate of mean global warming (Lee *et al.* 2021), there has been an increasing focus on harnessing renewable energy sources to reduce greenhouse gas emissions. Hydrokinetic energy is a renewable form of energy, where the kinetic energy of the flowing water is converted first into mechanical energy and then into electrical energy. Unlike traditional hydropower systems, which require the construction of dams, reservoirs, or diversion channels, hydrokinetic systems use turbines, generators, and other devices, which are placed directly into the flowing water in order to extract energy. As a result, it can be installed even in the most remote and extreme locations depending on the necessity and ease of installation. For identifying potential locations for hydrokinetic power extraction, it is important first to develop detailed datasets and estimates of available resources based on observed streamflow records, targeted hydrologic and hydraulic simulation experiments, or analysis of remotely sensed datasets. Such information, particularly for high latitudes, is generally not readily available.

Selected global to regional scale studies that have investigated the hydrokinetic potential utilizing observed streamflow, numerical modeling, and simulation techniques, and characteristics of various hydrokinetic energy systems and their feasibility for the Arctic regions are discussed below. At the global scale, Ridgill *et al.* (2021) assessed available riverine hydrokinetic resources using GRADES, a modeling system that incorporates the variable infiltration capacity land surface model (Liang *et al.* 1994) at 0.25° resolution and the routing application for parallel computation of discharge (David *et al.* 2011) with the MERIT-Hydro version 0.0 dataset (multi-error-removed-improved-terrain global hydrography data set; Yamazaki *et al.* 2019). They estimated the global resources to be of the order of $58,400 \pm 109$ TWh/year, which also demonstrated the high hydrokinetic potential of the North American continent. Although this study provides useful insights, the 25 km resolution, which is suitable for global-scale assessment, is too coarse for detailed site-specific analysis required for turbine installation.

At a regional level, the Underwood & McLellan group (1980) conducted one of the earliest Canada-wide assessments of hydropower potential based on observed streamflow data. As this study used data available prior to the 1980s, the analysis focused mainly on large rivers but suggested potential for hydrokinetic power in river reaches with flow greater than $450 \text{ m}^3/\text{s}$. Building up on the methodology used by the Underwood and McLellan (UMA) group, a similar study was conducted in the USA by Miller *et al.* (1986) for the US Department of Energy, focusing on the river reaches with mean flows greater than $113 \text{ m}^3/\text{s}$ and flow velocity greater than 1.3 m/s . The methodology considered provided a conservative assessment of the hydrokinetic power, suggesting an estimated total mean annual power of 12.5 GW (i.e., 110 TWh/year of hydrokinetic energy), with the highest contributions being associated with western, northwestern, and Alaskan regions. Later, Jacobson (2012) expanded this study to reaches with mean flows greater than $28 \text{ m}^3/\text{s}$. They reported technically recoverable hydrokinetic energy of up to 119.9 TWh/year, indicating an approximate 9% increase compared to the estimate provided in Miller *et al.* (1986). However, they could not validate their results due to the lack of empirical data from existing hydrokinetic energy conversion systems. Duvoy & Toniolo (2012) and Toniolo *et al.* (2010) studied the hydrokinetic potential of two river reaches in Alaska to assess the suitability of an in-stream river turbine installation. Velocity outputs generated by an existing depth-integrated two-dimensional hydrodynamic numerical model CCHE2D (Jia & Wang 2001; Zhang 2018), coupled with HYDROKAL (hydrokinetic calculator), were used to compute the instantaneous power density and identify potential installation sites for hydrokinetic power extraction. However, the employed model had difficulty in representing the helical flows, which developed on the outer slopes of river bends. For the Canadian high-latitude regions, although many studies have looked at streamflow characteristics (e.g., Su *et al.* 2005; Poitras *et al.* 2011; Clavet-Gaumont *et al.* 2013; Huziy *et al.* 2013; Teufel & Sushama 2021), very few studies have focused on hydrokinetic potential. Recently, Teufel & Sushama (2022b) did a preliminary analysis of hydrokinetic potential over Canada, including the high-latitude regions, for the current climate, by considering outputs from a coarse resolution regional climate modeling system. This study highlighted the need for high-resolution climate model outputs for better estimation of hydrokinetic potential.

Irrespective of the approach adopted for assessing the hydrokinetic potential globally or regionally for the historical periods, it is also important to consider the impact of future climate change, especially on streamflow regimes, magnitudes, and velocities, as these are the most important factors that determine hydropower potential. Teufel & Sushama (2021) studied the Canadian rivers using an ensemble of regional climate model (RCM) simulations and found mostly increases in the median annual streamflow for the Canadian Arctic region for the Representative Concentration Pathway 8.5 scenario. A previous RCM-based study by Poitras *et al.* (2011), for the Special Report on Emissions Scenarios (SRES) A2 scenario, also reported future increases in mean annual streamflow for the Arctic basins Mackenzie and Yukon. Climate change impacts on streamflow were considered by Zhang *et al.* (2023) for four major pan-Arctic river basins, namely Mackenzie, Ob, Lena, and Yenisei basins, using machine learning models such as support vector regression, artificial neural network, and multi-variable regression under climate change scenarios SSP2-4.5 and SSP5-8.5, using data from five CMIP6 global climate models (GCMs) for the 2020–2100 period. Their results suggest increases in mean annual streamflow for the studied basins.

Over the years, various hydrokinetic energy conversion systems have been studied and tested to harness the hydrokinetic energy of the flowing water bodies. In some cases, the conversion of hydrokinetic energy to electrical energy through a turbine can operate at almost zero head (Balat 2006). However, the amount of energy that can be harnessed from the flow depends on the turbine's efficiency and the flow velocity necessary for the operation of a hydrokinetic device, which typically ranges from 1 to 2 m/s , but in some cases, it can be as low as 0.5 m/s , depending on the additional methods adopted (Johnson & Pride 2010). Considering the orientation of the rotor with respect to the direction of the flow, hydrokinetic turbines are classified broadly into horizontal axis turbines or axial flow turbines and vertical axis turbines (Khan *et al.* 2009). Several deployments over the past decade, including the EVG-005H in Ruby, Alaska; the EVG-025H in British Columbia, Canada; and the Riverlution turbine in Alberta, Canada, adopted the vertical axis turbines, such as the H-Darrieus or Squirrel cage Darrieus (straight-bladed) turbines for river-based applications over the horizontal axis turbines, as they do not require a yaw mechanism, are quieter in operation, and are simple in design with the possibility to design a turbine with a diameter larger than the depth of the river in shallow rivers to generate higher power (Saini & Saini 2019; Khan *et al.* 2022). However, in cold regions, many cold weather operational adjustments are required, such as heating of the gearbox oil and ice removal, which are important for the functioning of the device, as any component that pierces the water interface will accumulate ice through direct splashing and freezing or buildups through frazil ice processes (Woods 2017). Several studies have been conducted to improve the efficiency of turbines in different flow conditions. Guney (2011) and Khan *et al.* (2008) exemplified that emphasis was on enhancing the performance coefficient and tip speed ratio by incorporating duct augmentation, variable

pitch blade structures for vertical turbines, a flip wing mechanism, fixed-wing rotor, amongst other strategies. The power from a single hydrokinetic turbine is usually small, and thus the energy density can be increased by the installation of the turbines in arrays or farms (Balat 2006).

Due to limited and sporadic observational data in the higher latitudes, hydrological models can be employed to estimate streamflow. The conventional approach to studying climate change impacts on streamflow and power generation involves the use of hydrological model simulations driven by climate model outputs corresponding to selected emission scenarios. Interactive modeling of streamflow at several kilometers to sub-kilometers scale using a climate-hydrology integrated modeling approach is also starting to emerge with recent advances in the areas of high-resolution modelling (e.g., Prein *et al.* 2015; Diro & Sushama 2019; Teufel & Sushama 2022a; b) and high-performance computing. Such fine resolutions help further improve the simulated streamflow due to better representation of surface characteristics and soil and landscape heterogeneities in the climate model. The objective of this study is to assess the hydrokinetic power potential in the Canadian Arctic using continuous streamflow sequences derived from ultra-high-resolution climate model simulations performed using a state-of-the-art regional climate model for both current and future climates.

The rest of the paper is structured as follows: Section 2 comprises a detailed description of the streamflow data and related climate and routing models, along with the methodology. Section 3 focuses on streamflow validation and discusses characteristics of estimated flows, flow velocities, and hydrokinetic power for the current 2001–2020 period. Projected changes to hydrokinetic power for the near-future 2021–2040 period are presented in Section 4. Section 5 discusses potential areas for hydropower extraction. Discussion and conclusions are provided in Sections 6 and 7, respectively.

2. STREAMFLOW DATA AND METHODOLOGY

2.1. Simulated and observed streamflow data and related models

In this study, streamflow estimates are obtained for the Canadian Arctic using a modified version of the cell-to-cell routing scheme, WATROUTE (Soulis *et al.* 2000; Teufel & Sushama 2021; Kouwen 2023), driven by runoff simulated by a regional climate model, the global environment multiscale (GEM) model (Côté *et al.* 1998), at 4 km resolution over a 748×700 grid points domain (Figure 1), covering Nunavut and adjoining regions. These streamflow estimates are further utilized in the estimation of hydrokinetic power potential.

The state-of-the-art regional climate model, GEM, solves non-hydrostatic, deep atmosphere dynamics with an implicit, two-time-level semi-Lagrangian numerical scheme. In the horizontal, the model uses a regular latitude–longitude grid with Arakawa C staggering and a rotated pole configuration such that the domain is approximately centered on the equator to minimize changes in grid spacing across the domain. In the vertical coordinate, following Girard *et al.* (2014), Charney–Phillips staggering is used. The radiation scheme is represented by the correlated K solar and terrestrial radiation of Li & Barker (2005) and the planetary boundary layer scheme follows Benoit *et al.* (1989) and Delage (1997). The double-moment microphysics scheme of Milbrandt & Yau (2005) is used for condensation processes. In addition to the large-scale precipitation schemes, the model includes the deep convection scheme of Kain & Fritsch (1990) and the shallow convection based on Bélair *et al.* (2005). As discussed in Teufel & Sushama (2022a), the use of convection parameterization for ~ 3 –8 km grid spacing is still a topic of debate and considered a gray zone, as convection is neither fully resolved nor can it be assumed to be smaller than the grid box spacing (Gerard *et al.* 2009).

The land processes in GEM are represented by the Canadian Land Surface Scheme (Verseghy 2011). Given the importance of permafrost in the study domain, the scheme uses a 60 m deep soil layer configuration, consisting of 26 layers of varying thicknesses: 0.1, 0.2, 0.3, 0.4, 0.5 ($\times 10$), 1.0, 3.0, and 5.0 ($\times 10$) m.

WATROUTE is based on the routing algorithm of the WATflood-distributed hydrological model (Kouwen *et al.* 1993; Soulis *et al.* 2000). In the original version of WATROUTE, routing through the digital river network is performed using a single surface reservoir. The modified version of WATROUTE used in this study includes a groundwater reservoir modeled as a linear reservoir as proposed in Sushama *et al.* (2004). Detailed information on the model formulation can be found in Teufel & Sushama (2022b).

The flow directions of rivers, channel length, and slopes that are required by WATROUTE are obtained from the Hydrological Data and Maps based on Shuttle Elevation Derivatives at Multiple Scales (HydroSHEDS) database (Lehner *et al.*

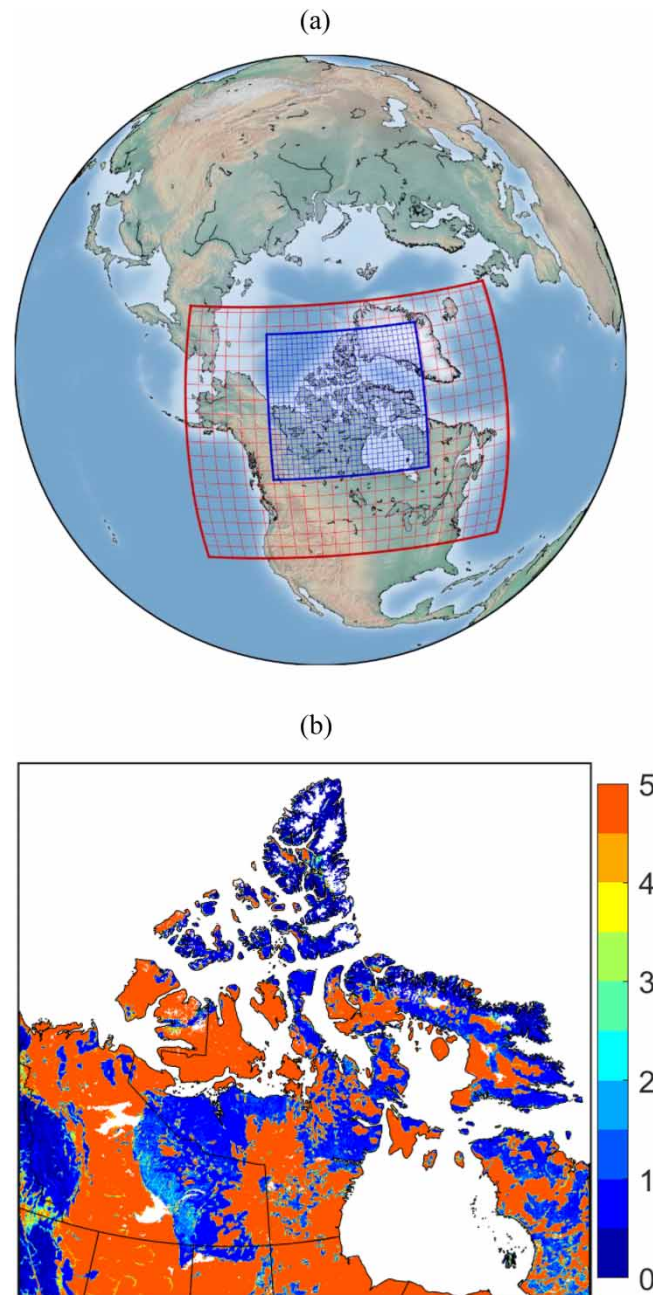


Figure 1 | (a) GEM experimental domains at 4 km (in blue) and 10 km (in red) resolutions; the downscaled CanESM2 simulation at 10 km resolution is used to drive the 4 km GEM transient climate change simulation. (b) Depth to bedrock at 4 km resolution in meters.

2008). The primary sources of data used in the development of HydroSHEDS are the digital elevation model from National Aeronautics and Space Administration (NASA)'s Shuttle Radar Topography Mission (SRTM), with ancillary data sources such as the SRTM Water Body Data, the river networks of the Digital Chart of the World (ESRI 1993), and Arc World (ESRI 1992), and the Global Lakes and Wetlands Database (Lehner & Döll 2004). The processing steps of generating HydroSHEDS are available in the technical documentation by Lehner *et al.* (2013). As the SRTM elevation data are not available beyond 60° N latitude, DEM from the HYDRO1k database (USGS 2000) is used to complete the hydrographic data and thus to obtain full global coverage of the drainage networks and sub-basin delineations. The flow direction from HydroSHEDS is upscaled to 4 km resolution following Huziy *et al.* (2013) and Döll & Lehner (2002).

2.2. Methodology

Two streamflow simulations are considered in this study. The first spans the period from 2001 to 2020 and is derived from runoff simulated by the GEM model at 4 km resolution using the WATROUTE routing scheme. Here, the GEM simulation is driven by ‘perfect boundary conditions’, namely, the European Centre for Medium Range Weather Forecasts ERA5 reanalysis (Hersbach *et al.* 2020) over the domain shown in Figure 1(a). The initial soil conditions for this simulation are based on a pan-Arctic GEM simulation driven by ERA-Interim (Teufel *et al.* 2019), while the atmospheric initial conditions are specified from ERA5. This simulation, hereafter referred to as GEM_ERA5, is used for validation purposes. The second streamflow simulation, spanning from 2001 to 2040, is derived from a transient climate change GEM simulation driven by the Canadian Earth System Model (CanESM2) under the Representative Concentration Pathway (RCP) 8.5 emission scenario (Riahi *et al.* 2011); this simulation is denoted as GEM_CanESM2, referencing the specific period of interest, i.e., ‘current’ for 2001–2020 and ‘future’ for 2021–2040. When driven by CanESM2, GEM simulations are initially downscaled to 10 km resolution (the outer domain shown in Figure 1(a)); the outputs (temperature, wind, humidity, surface pressure, and geopotential height fields) from which are used as the lateral boundary conditions for the ultra-high-resolution GEM simulation over the inner domain at 4 km resolution. The initial conditions for the 4 km GEM simulation are obtained from the 10 km GEM simulation driven by CanESM2.

For validation purposes, streamflow derived from GEM_ERA5 runoff is compared with streamflow observations from HYDAT, which is the national archival database maintained by Environment and Climate Change Canada. Additionally, the map of Nunavut’s water management areas is utilized to identify 65 basins in Nunavut (Nunavut Water Board 2014) (see Figure 2) to contextualize results and discussion. The scarcity of available observed streamflow data in the Canadian Arctic poses a significant limitation for performing a detailed evaluation of model simulations. Of the 187 hydrometric monitoring stations available over the study domain, only six have consistent data for at least 3 years within the 2001–2020 period, along with comparable drainage areas. These stations, shown in Figure 2, used for validating model simulated flows, are located at the outlets of the Queen Maud Gulf (Basin ID: 30) and Back (Basin ID: 31) basins toward the central-north, and the Thelon (Basin ID: 5) basin flowing into the Hudson Bay. Although the Mackenzie basin is not entirely covered by the study domain, three of its sub-basins (Basin ID: M1 to M3; Figure 2) that have their entire accumulation area within the study domain are also considered in the analysis. Basins located in northern Quebec that fall within the GEM domain are not included in the analysis, as the focus is on Nunavut and adjoining regions. The accumulated drainage areas of the studied basins are also shown in Figure 2 to illustrate drainage patterns as water moves from source areas to the outlets of basins.

The available hydrokinetic power P_k is estimated from the simulated streamflow at 4 km resolution as $P_k = (\rho/2)AV^3$, where ρ is the fluid density (considered as 1,000 kg/m³), and A and V are the cross-sectional area and flow velocity, respectively. The power captured by a hydrokinetic turbine is a fraction of that estimated using this equation, as it also depends on the swept area of the rotor and the performance coefficient of the turbine, which vary with the turbine and modifications considered.

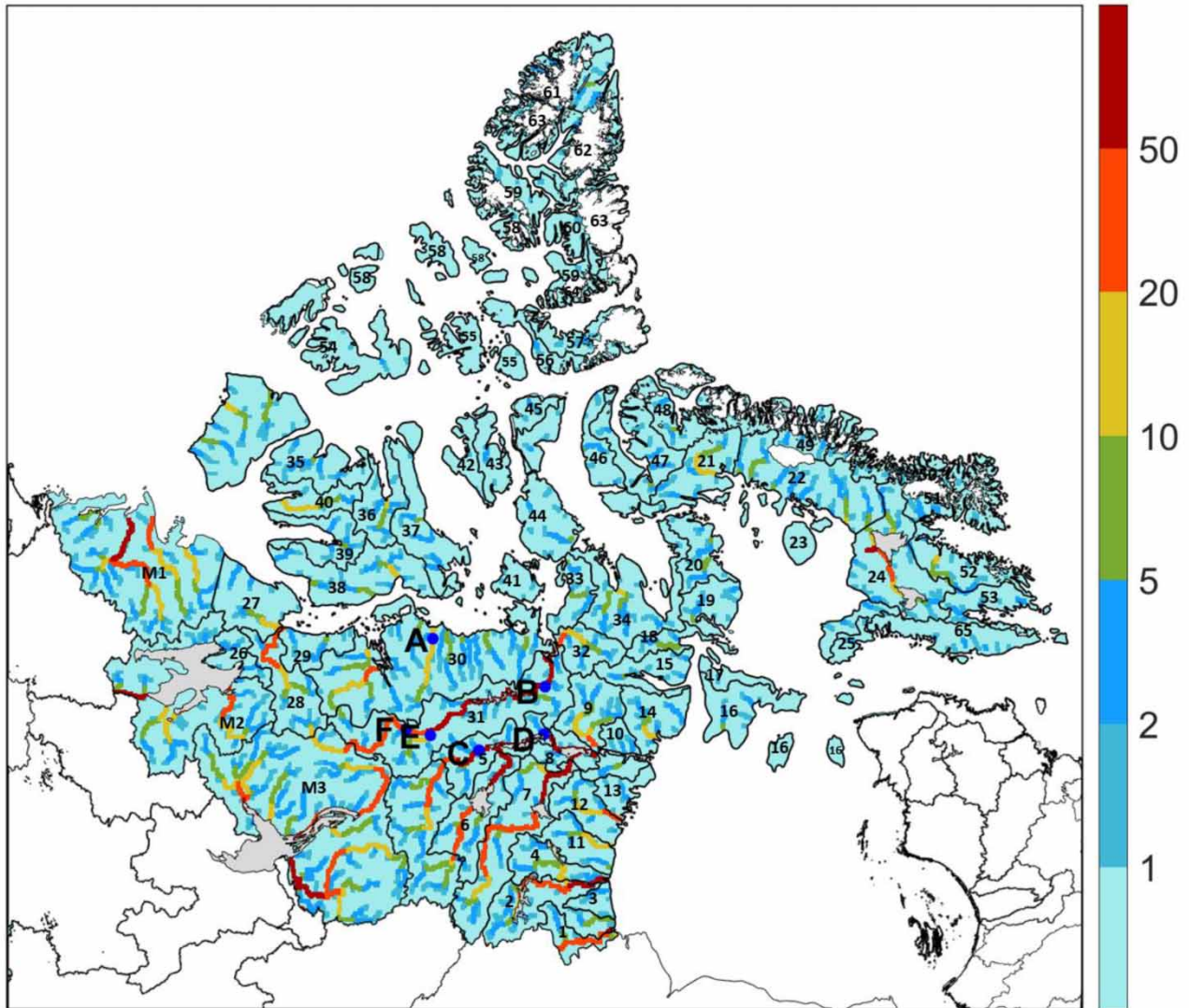
To identify river reaches suitable for hydropower extraction, a velocity threshold of 1.5 m/s is considered, following the guidelines for the practical operation of hydrokinetic turbines (Johnson & Pride 2010). The number of days with velocity greater than this threshold is estimated, which could be useful in decision-making. Although other criteria, including site characteristics, can be considered, this study focuses only on the velocity threshold.

Projected changes to streamflow, flow velocities, and hydrokinetic power are obtained by comparing the future 2021–2040 period with the current 2001–2020 period of GEM_CanESM2-based WATROUTE simulations.

3. STREAMFLOW, VELOCITY, AND HYDROPOWER CHARACTERISTICS AND VALIDATION

Before discussing the validation of streamflow estimates, which is an important component of this study, GEM_ERA5 simulated runoff fields for the 2001–2020 period are discussed. The spatial patterns of surface runoff simulated by GEM_ERA5, shown in Figure 3(a) for various seasons, show that the region of high values migrates from south to north from spring to summer. The highest magnitudes of seasonal mean runoff of up to 7 mm/day are noted during summer, primarily due to a combination of rainfall and/or snow/glacier melt for these regions. The GEM_CanESM2 simulation for the same period also shows very similar patterns (Figure 3(b)), suggesting minimal boundary-forcing errors, i.e., errors associated with boundary-forcing data errors; negative boundary-forcing errors of up to 1 mm/day are noted for the southern and central regions

$\times 10^3 \text{ km}^2$



- | | | | | |
|------------------------|---------------------------|-------------------------------|------------------------------------|---------------------------------|
| 1. Seal | 16. Hudson bay Islands | 31. Back | 46. W Brodeur Peninsula | 61. Arctic Ocean and Lincon Sea |
| 2. Thlewiaza | 17. N Southampton islands | 32. Back - Hayes (Nunavut) | 47. Admiralty Inlet | 62. NE Ellesmere island |
| 3. Geillini | 18. Repulse Bay | 33. Rasmussen Victoria Island | 48. Eclipse Sound | 63. SE Ellesmere Island |
| 4. Than - anne | 19. Barrow | 34. Gulf of Boothia | 49. SW Baffin Bay | 64. S Ellesmere Island . |
| 5. Thelon | 20. Kingora | 35. NW Victoria Island | 50. NW Davis Strait | 65. Hudson Strait -N and W |
| 6. Dubawnt | 21. Gifford | 36. Hadley Bay | 51. N Cumberland Sound | M1 . Mackenzie Main Sub - basin |
| 7. Kazan | 22. Macdonald | 37. E Victoria Island | 52. S Cumberland Sound | M2 . Mackenzie Main Sub - basin |
| 8. Baker Lake | 23. Prince Charles Island | 38. S Victoria Island | 53. Frobisher Bay | M3 . Slave Sub - basin |
| 9. Quoich | 24. Kodkdjuak | 39. Prince Albert Sound | 54. Melville Island | |
| 10. Chesterfield inlet | 25. Aukpar | 40. Minto Inlet | 55. Bathrust and Cronwallis Island | |
| 11. Maguse | 26. Great Bear | 41. King William Island . | 56. W Devon Island | |
| 12. Freguson | 27. Amundsen Gulf | 42. W Prince of Wales Island | 57. E Devon Island | |
| 13. Wilson | 28. Coppermine | 43. E Prince of Wales Island | 58. Sverdrup Islands | |
| 14. Lorillad | 29. Coronation Gulf | 44. W Somerset island | 59. Nansen and Eureka Sounds | |
| 15. Wager Bay | 30. Queen Maud Gulf | 45. E Somerset Island | 60. Greely Fiord | |

Figure 2 | Location of HYDAT stations (A–G; blue dots) used for validation and the study region comprising of 65 Nunavut basins (Source: Nunavut Waters Regulations) along with three sub-basins of the Mackenzie basin (M1 to M3). The IDs and names of the basins are listed above, where: NE – North Eastern, NW – North-Western, SW – South-Western, SE – South-Eastern, N – North, S – South, E – East and W – West. The accumulated drainage area is shown in color.

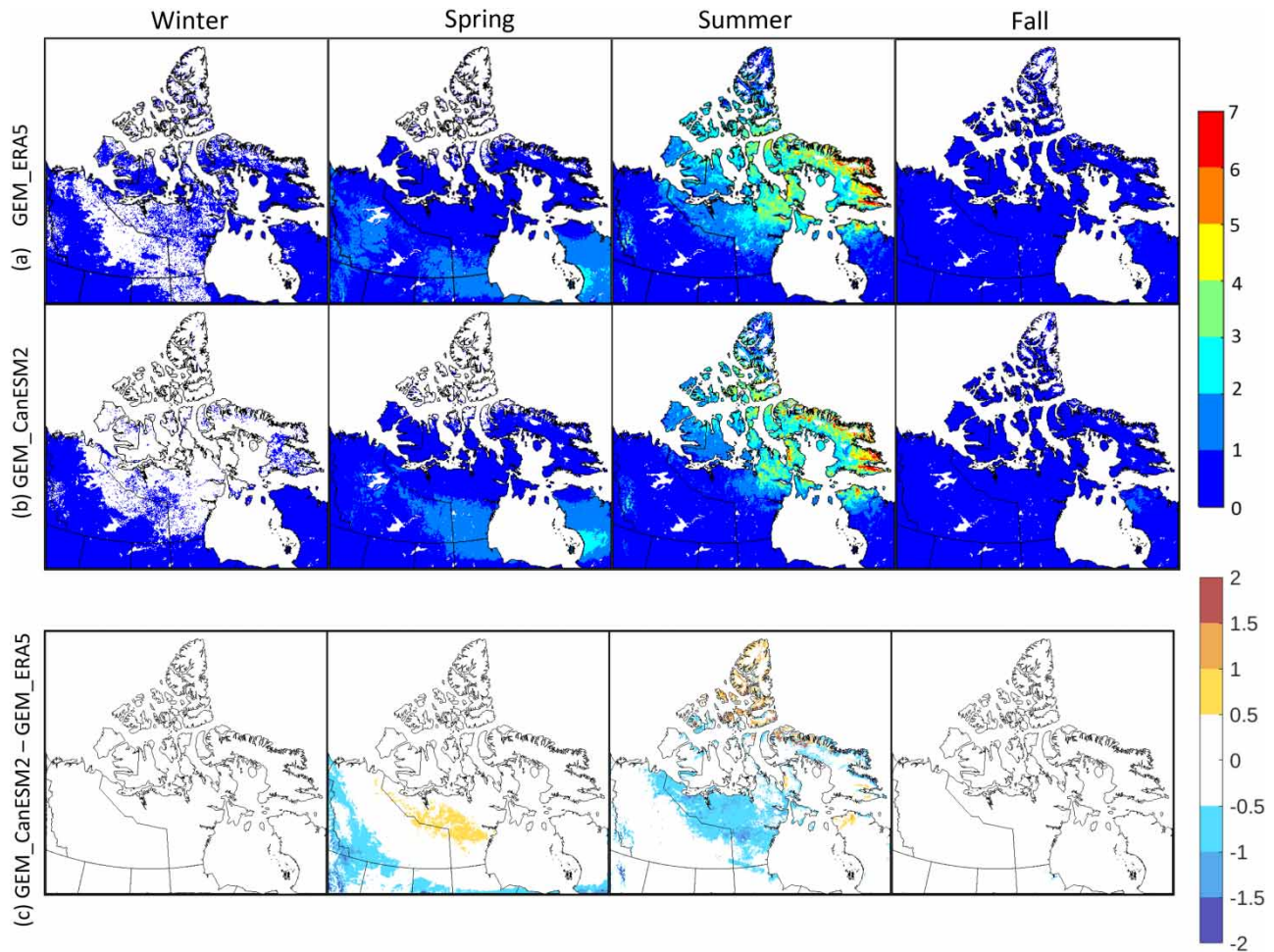


Figure 3 | Spatial plots of mean seasonal surface runoff (mm/day) for (a) GEM_ERA5, (b) GEM_CanESM2, and (c) their differences for the 2001–2020 period.

during spring and summer, respectively. Some positive boundary-forcing errors in the same range are also noted during spring for the central regions. Bottom drainage patterns (Figure 4) suggest an absence of drainage for continuous permafrost regions, except where bedrock is very close to the surface, with maximum drainage contributing cells noted in fall. GEM_CanESM2 simulated drainage when compared with GEM_ERA5 suggests some differences, particularly for summer and fall (Figure 4). In GEM_CanESM2, the regions with drainage extend further north in summer compared to GEM_ERA5. This is partially due to the warm bias in the driving CanESM2 data, which, as reported in Teufel & Sushama (2022a), is also reflected in the near-surface and soil temperatures in GEM_CanESM2. Teufel & Sushama (2022a) had considered the same GEM simulations as in this study and provided extensive validation of GEM fields, including 2-m temperature, soil temperature, precipitation, and wind fields, which were all found to agree very well with observed data. Since streamflow is the most important variable that influences hydrokinetic power, validation of simulated streamflow characteristics is presented next.

The mean annual hydrograph, observed and simulated, shown in Figure 5 for six selected stations, has high flows generally occurring during the May to August period, given their northerly location, and is primarily snowmelt driven. Low flows occur during late winter or early spring as expected for these northerly regions. The timing of peak flows for the GEM_ERA5-based hydrograph agrees with that observed (see Figure 5) in most cases, indicating the ability of GEM to simulate the key processes that influence streamflow in the region. However, a slight underestimation of observed peak flow magnitudes can be noted in Figure 5. These differences can be partly attributed to the underestimation of snow water equivalent (SWE) in GEM simulations (Teufel & Sushama 2021). The GEM_CanESM2-based streamflow magnitudes are overall similar to that of GEM_ERA5, although some negative boundary-forcing errors can be noticed for the peak flows, which can be associated

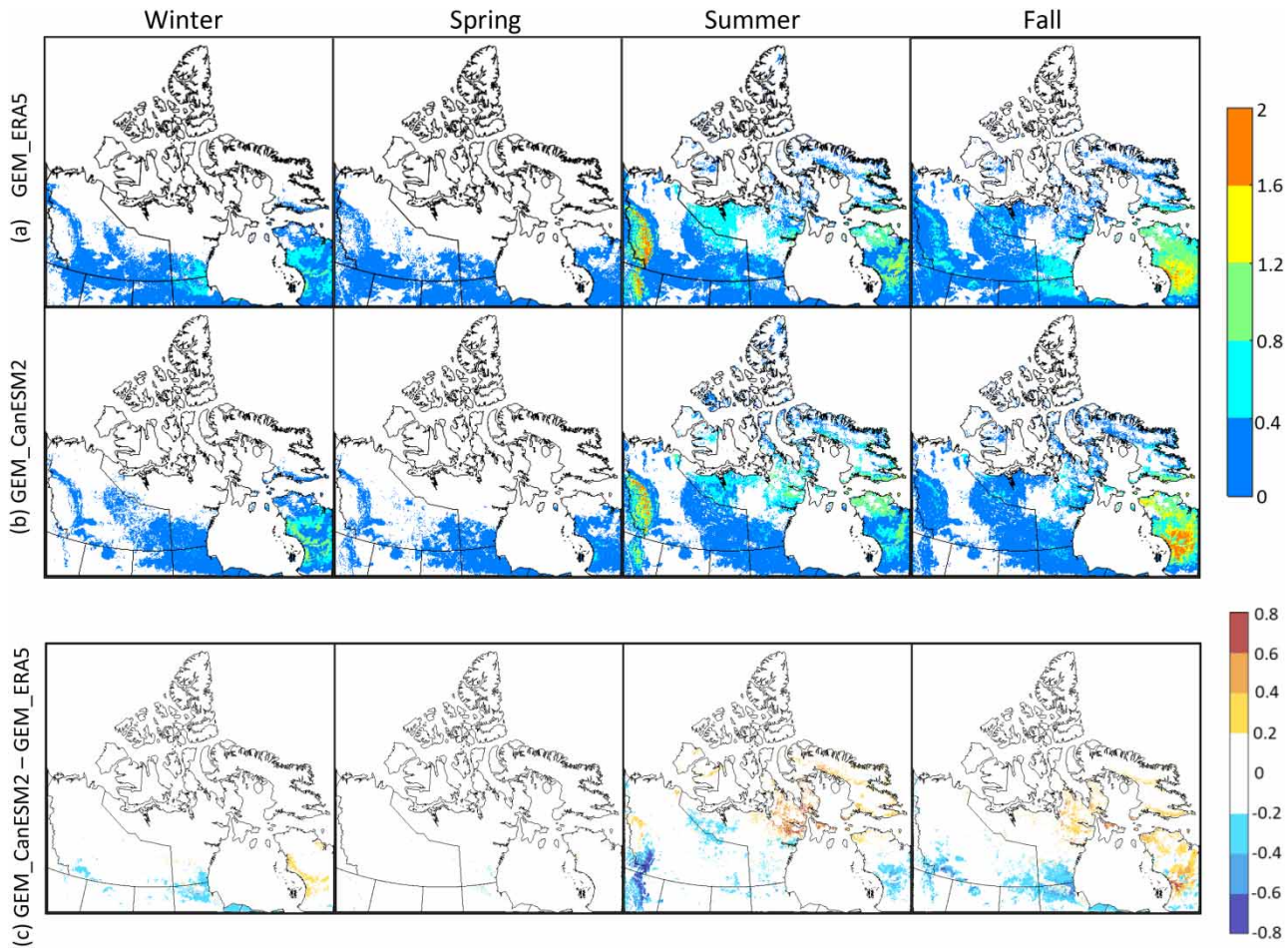


Figure 4 | Spatial plots of mean seasonal bottom drainage (mm/day) for (a) GEM_ERA5, (b) GEM_CanESM2, and (c) their differences for the 2001–2020 period.

with the negative boundary-forcing errors in SWE (Teufel & Sushama 2021). Despite these differences, the modeled streamflows capture the main features of the observed hydrograph with Nash–Sutcliffe efficiency coefficients in the 0.92–0.96 and 0.85–0.92 ranges for GEM_ERA5 and GEM_CanESM2, respectively, suggesting good performance overall, giving confidence in the simulations.

The spatial plots of simulated mean seasonal streamflow estimates based on GEM_ERA5 shown in Figures 6(a) and S1(a) are consistent with the runoff and drainage estimates discussed earlier. The streamflow magnitudes are higher during the spring and summer seasons for southern and northern basins, respectively, corresponding to the snowmelt period. The maximum flows in the Nunavut basins are noted in the 1,000–10,000 m³/s range, with the highest values noted at the basin outlets (along the Hudson Bay and the Arctic). As for the streamflow based on GEM_CanESM2, they are similar to those based on GEM_ERA5, with some negative and positive boundary-forcing errors noted for the southern to central basins, depending on the season (Figures 6(c) and S1(c)).

The flow velocity (Figures 7(a) and S2(a)) shows higher magnitudes during summer in those regions where streamflow is also estimated to be higher. The magnitude of streamflow velocity is one of the important parameters that is used to quantify the amount of hydrokinetic power that can be generated at a particular cross-section of the river or stream channel. The highest magnitude of flow velocity above 2 m/s is noted at the outlets of the major basins; however, the 1.5–2 m/s range is noted along the main tributaries of the Back basin (Basin ID: 31), Back_hayes (Basin ID: 32), and Thelon basin (Basin ID: 5) located in central Nunavut and along the Seal basin (Basin ID: 1) and Thlewaiza basin (Basin ID: 2) in southern Nunavut. The GEM_CanESM2-based velocity patterns are overall similar to those based on GEM_ERA5, with differences being less

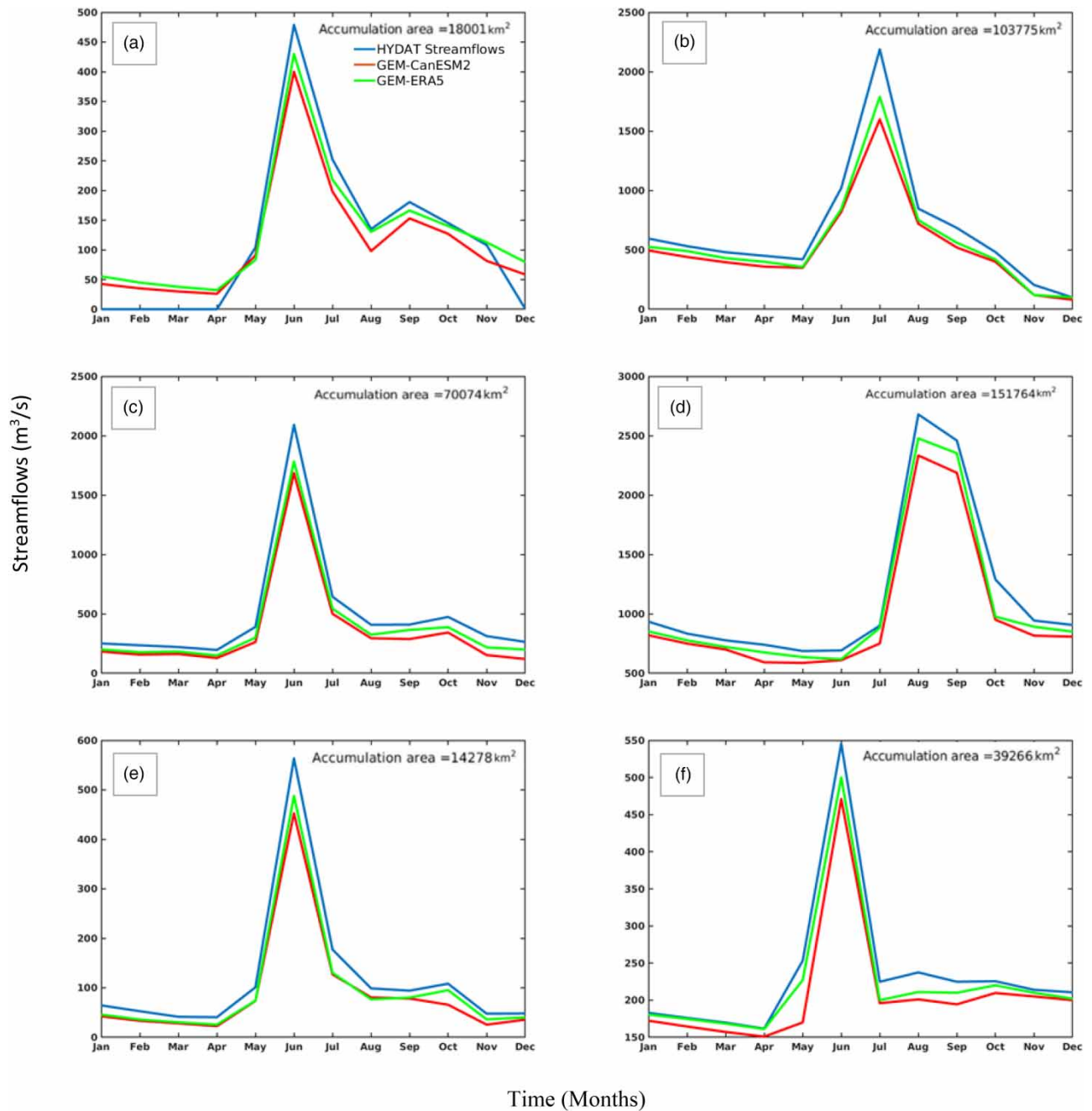


Figure 5 | Mean annual hydrograph for HYDAT (blue), GEM_CanESM2 (red), and GEM_ERA5 (green), for the 2001–2020 period, at six station locations shown in Figure 2.

than 0.2 m/s over most of the domain of interest. The boundary-forcing error patterns for velocity are similar to those for streamflow.

The spatial plots of hydrokinetic power potential shown in Figures 8 and S3 are consistent with the spatial patterns of flow velocity and streamflow. Higher power potential is noted near the outlet of the rivers flowing into the Queen Maud Gulf, Coronation Gulf in central Nunavut, and Hudson Bay in the east. Some basins belonging to the Nunavut province, such as the Back (Basin ID: 31), Back-Hayes (Basin ID: 32), and Queen Maud Gulf (Basin ID: 30) basins flowing into the Rasmussen Basin along the Arctic coast in central Nunavut, Baker Lake (Basin ID: 8), Thelon (Basin ID: 5), and Quoich (Basin ID: 9)

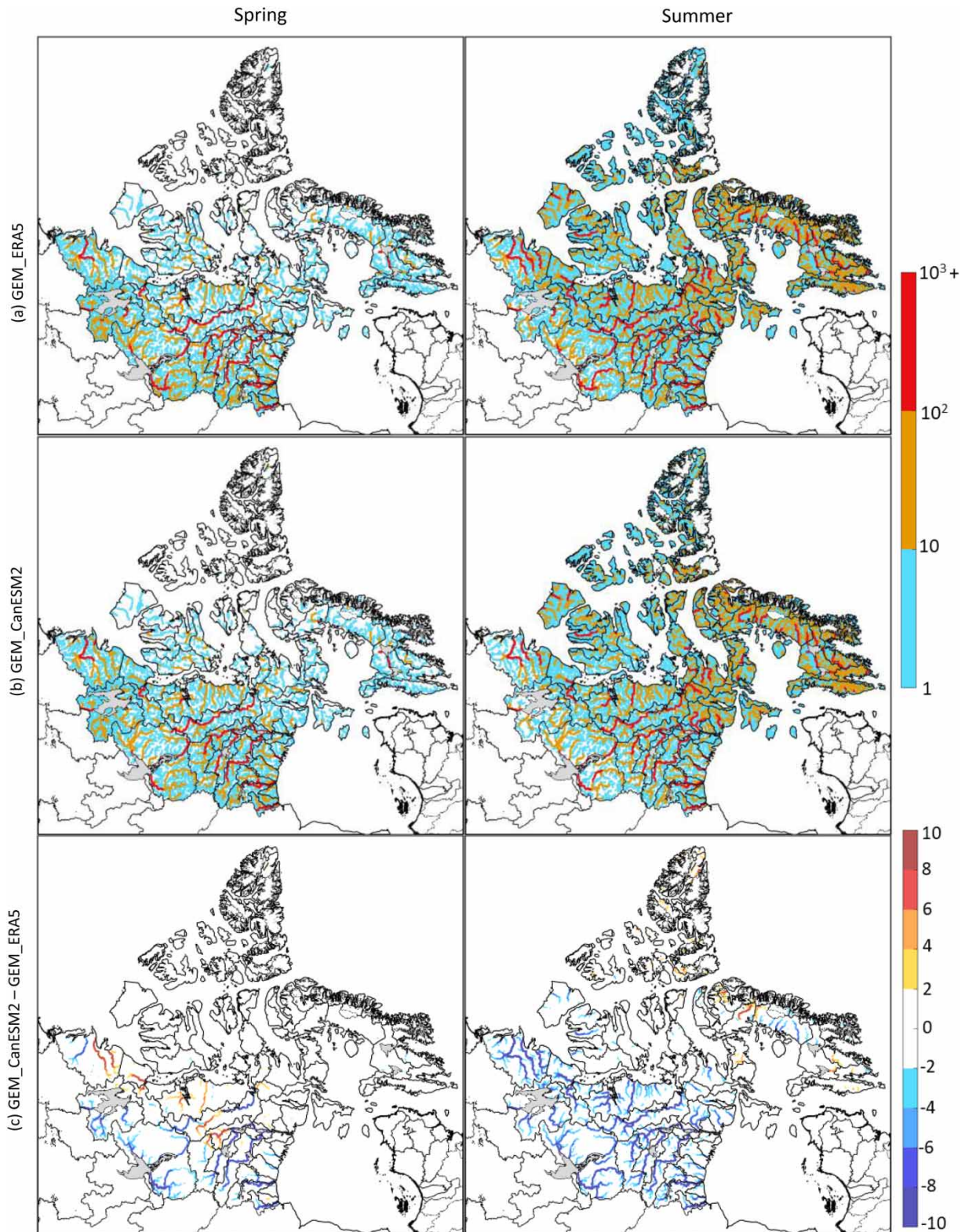


Figure 6 | Spatial plots of mean spring and summer flows (m³/s) for (a) GEM_ERA5, (b) GEM_CanESM2, and (c) their differences for the 2001–2020 period.

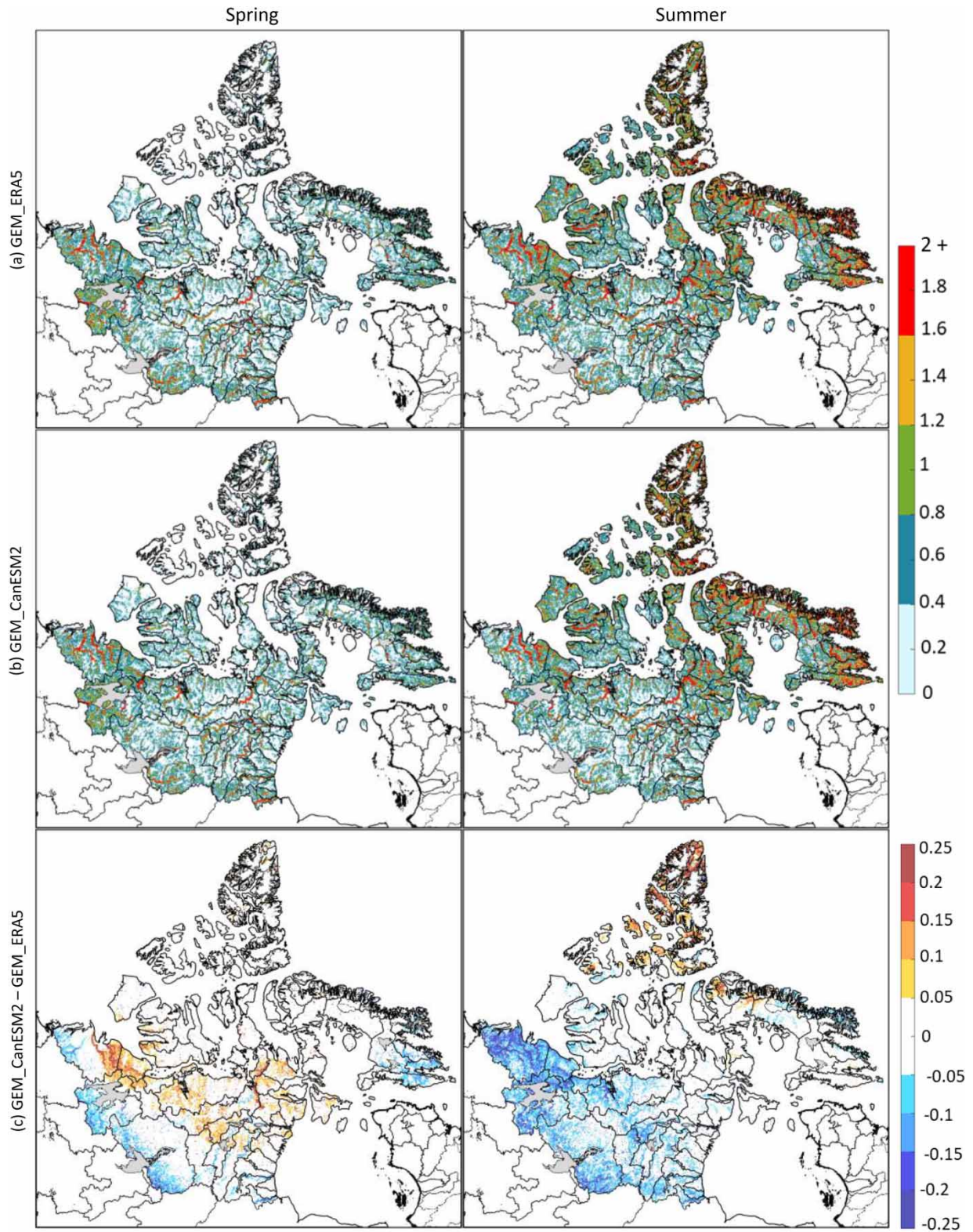


Figure 7 | Spatial plots of mean spring and summer flow velocities (m/s) for (a) GEM_ERA5, (b) GEM_CanESM2, and (c) their differences for the 2001–2020 period.

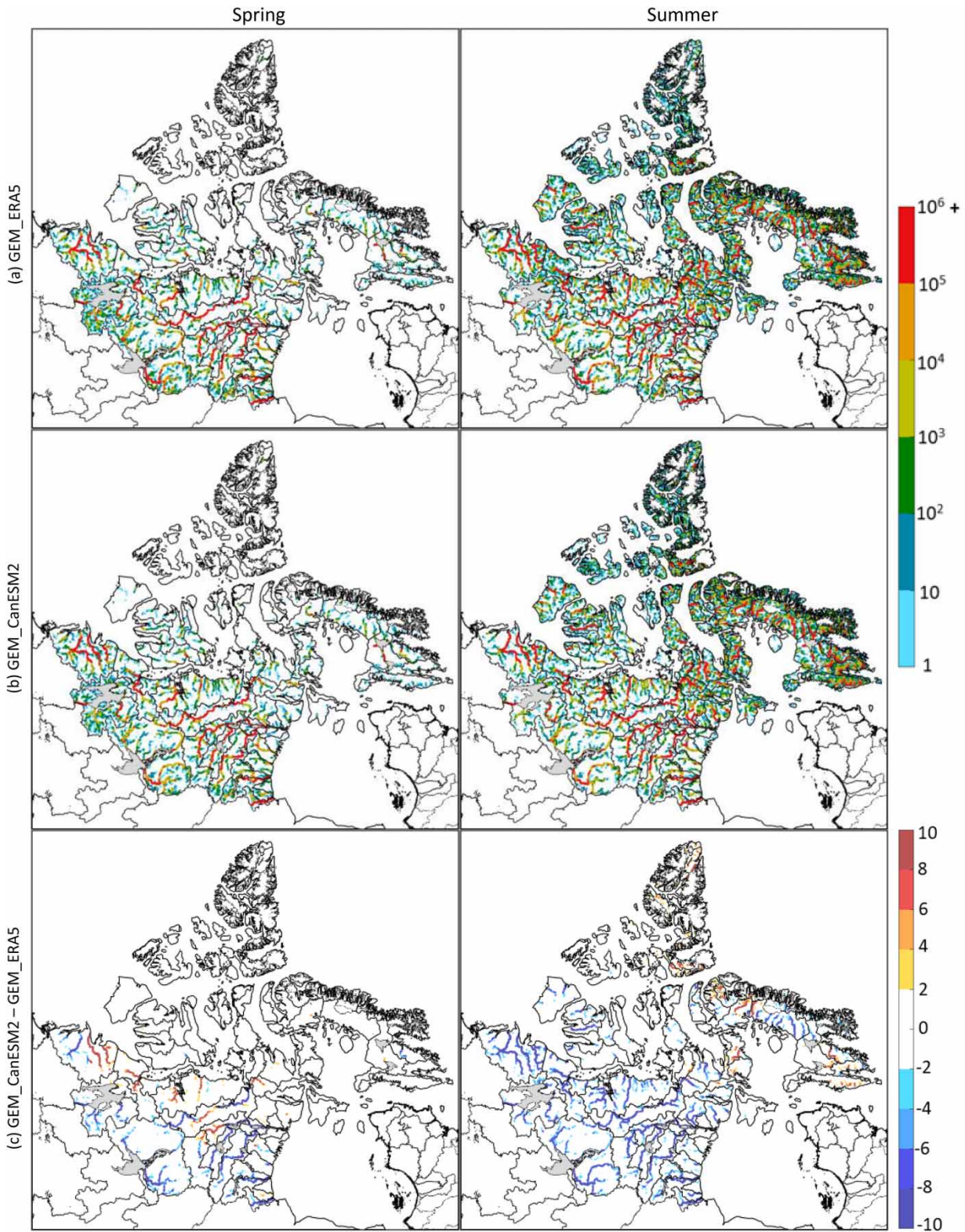


Figure 8 | Spatial plots of mean spring and summer hydrokinetic power (kW) for (a) GEM_ERA5, (b) GEM_CanESM2, and (c) their differences for the 2001–2020 period.

basins flowing through the Chesterfield inlet across the eastern region into the Hudson Bay, show high potential for power generation continuously throughout the year. The Than-anne (Basin ID: 4), Thlewaiza (Basin ID: 2), and Seal (Basin ID: 1) in southeastern Nunavut flowing into the Hudson Bay similarly also show high potential for hydrokinetic power extraction. With higher flow velocity values in summer, the hydrokinetic potential is also higher during these months compared to the rest of the year. Consistent with the velocity results, GEM_CanESM2-based hydrokinetic power estimations exhibit lower values compared to those based on GEM_ERA5, suggesting negative boundary-forcing errors, particularly for the southern parts of the domain, and positive boundary-forcing errors for the northernmost regions, especially during the summer season. However, these differences are in the 2–10 kW range. Since projected changes are assessed by comparing the future and current periods of streamflow-related estimates based on the GEM_CanESM2 simulations, careful interpretation is required for regions that exhibit higher boundary-forcing errors.

4. PROJECTED CHANGES TO STREAMFLOW, VELOCITY, AND HYDROPOWER

Before presenting projected changes to streamflow, projected changes to runoff and drainage variables are presented. The projected changes to surface runoff indicate a potential increase in runoff during the summer season for the northern regions (Figure 9(a)). Bottom drainage shows clear increases in summer, especially for regions where the bedrock table is closer to the surface (Figure 9(b)). This increase is attributed to higher temperatures in a warmer climate and related increases in the active layer thickness (which is the surface soil layer subject to the annual freeze-thaw cycle), deeper than the bedrock table.

Projected changes to streamflow observed within the study basins are modest in magnitude and exhibit a dipole pattern. Increases are noted particularly for the northern regions (Figures 10(a) and S4(a)), with a maximum increase of $10 \text{ m}^3/\text{s}$ noted during summer. The southern regions show decreases, primarily due to the reduced surface runoff contribution in the future climate, associated with decreases in snow depth in winter months and decreases in water yield (precipitation minus evapotranspiration) (figures not shown). The projected increases in streamflow for the northern regions are primarily due to the projected increases in snow depth and increase in water yield during the warmer seasons. The anticipated projected changes to streamflow velocity align with the pattern observed for streamflow. The northernmost regions show

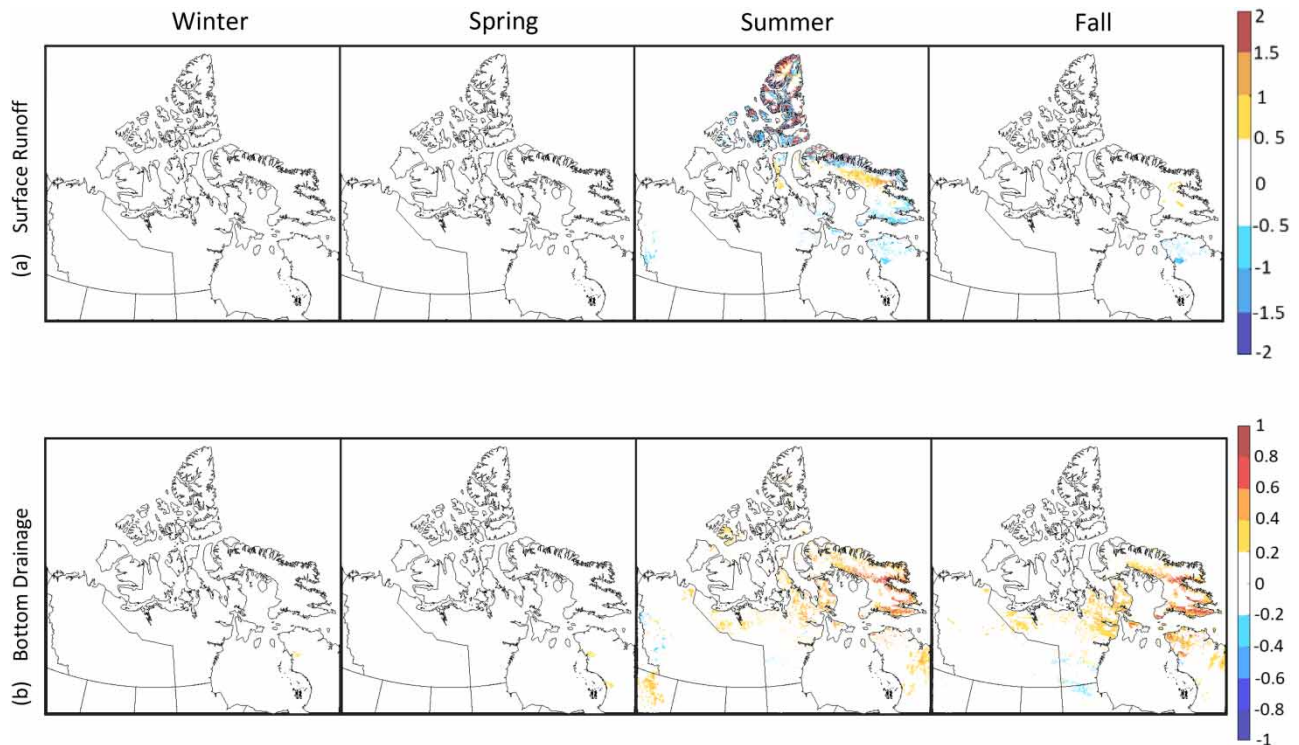


Figure 9 | Projected changes to (a) surface runoff and (b) bottom drainage in mm/day for the 2021–2040 period with respect to the 2001–2020 period.

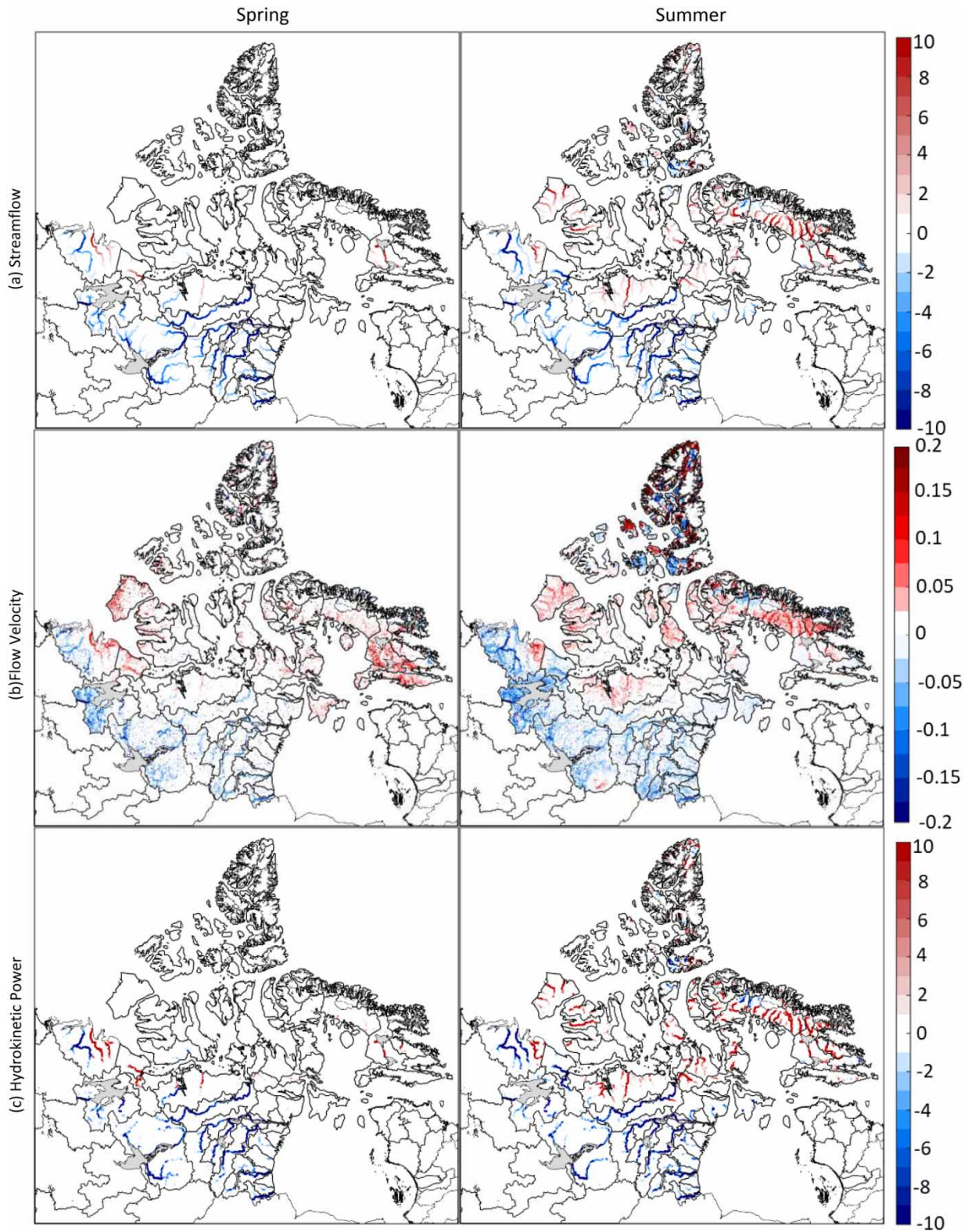


Figure 10 | Projected changes to mean spring and summer (a) streamflow (m^3/s), (b) flow velocity (m/s), and (c) hydrokinetic power (kW) for the 2021–2040 period with respect to the 2001–2020 period.

minor increments, up to a maximum of 0.2 m/s (middle panels of Figures 10 and S4). These increases are predominantly concentrated in regions located in the central and northern regions of Nunavut. The projected changes to the hydrokinetic power potential of the rivers exhibit similar dipole patterns as for flow velocity, with increases for the northern regions of Nunavut.

For regions where the current annual mean hydrokinetic power potential is in the 10^3 – 10^5 kW range, the projected changes are in the 0–4 kW range. Similarly, where the current power potential is in the 10^3 – 10^6 kW range, a change of up to 10 kW is noted. However, the highest change in the 100–500 kW range is noted for the regions where the current power potential is in the 10^6 – 10^9 kW range, which is at the outlets of the basins. Table 1 provides the list of the top 10 Nunavut basins with hydrokinetic power potential and their projected changes. The relatively modest changes noted are an expected scenario, as more prominent changes are anticipated toward the end of the 21st century under the RCP 8.5 scenario.

5. LOCATIONS FOR TURBINE INSTALLATION

As discussed in Section 2.2, to identify locations suited for hydrokinetic power extraction, i.e., for the installation of hydrokinetic conversion systems, the number of days wherein the flow velocity surpasses the critical threshold of 1.5 m/s is estimated. For the current 2001–2020 period, the number of days with flow velocity greater than 1.5 m/s is found to be in the 200–330 range for most of the main tributaries in the south and central basins (Figure 11), particularly the Back (Basin ID: 31) and Back-Hayes (Basin ID: 32) basins in central Nunavut, and the Seal (Basin ID 1), Than-anne (Basin ID 4), and Thlewaiza basins (Basin ID 2) in the southeast region of Nunavut.

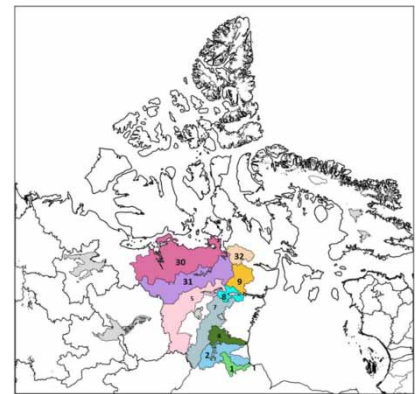
In the future 2021–2040 period, the number of days shows increases of up to 10 days for the northern basins, while decreases of the same order are noted for the southern basins (Figure 11(b)). These are consistent with the velocity patterns shown in Figures 10 and S4.

6. DISCUSSION

In this paper, hydrokinetic power potential is estimated for Nunavut and adjoining regions using an integrated climate-hydrology modeling approach at 4 km resolution for the 2001–2020 period, which is considered a surrogate for limited historical records. This physically sensible approach is adopted due to the severe lack of hydrometric station-based observations and to produce estimates of hydrokinetic power potential at reasonably fine spatial resolutions throughout the region to support optimal siting of hydrokinetic power extraction systems. A triangular cross-section of the river channel is assumed when using WATROUTE. This choice simplifies the calculations required for estimating hydraulic properties, such as flow areas and hydraulic radius, and reduces the need for detailed cross-sectional and profile data. This approach is particularly beneficial when dealing with large basins, such as those considered in this research, where data collection is both challenging and

Table 1 | The basin ID and names of Nunavut basins with the highest hydrokinetic power potential in descending order are shown in columns 1 and 2

Potential basins		Hydrokinetic power (kW)	
Basin ID	Names	2001–2020	2021–2040
8	Baker Lake	794,328	794,128
5	Thelon	100,000	99,654
1	Seal	100,000	99,600
31	Back	79,433	79,203
7	Kazan	10,000	9,800
32	Back-Hayes	3,163	3,255
2	Thlewaiza	3,163	3,150
4	Than-anne	1,000	880
9	Quoich	759	769
30	Queen Maud Gulf	501	531



Note. The third column shows the hydrokinetic power for the grid cells with median values for respective basins for the current 2001–2020 period and the fourth column shows their future values for the 2021–2040 period.

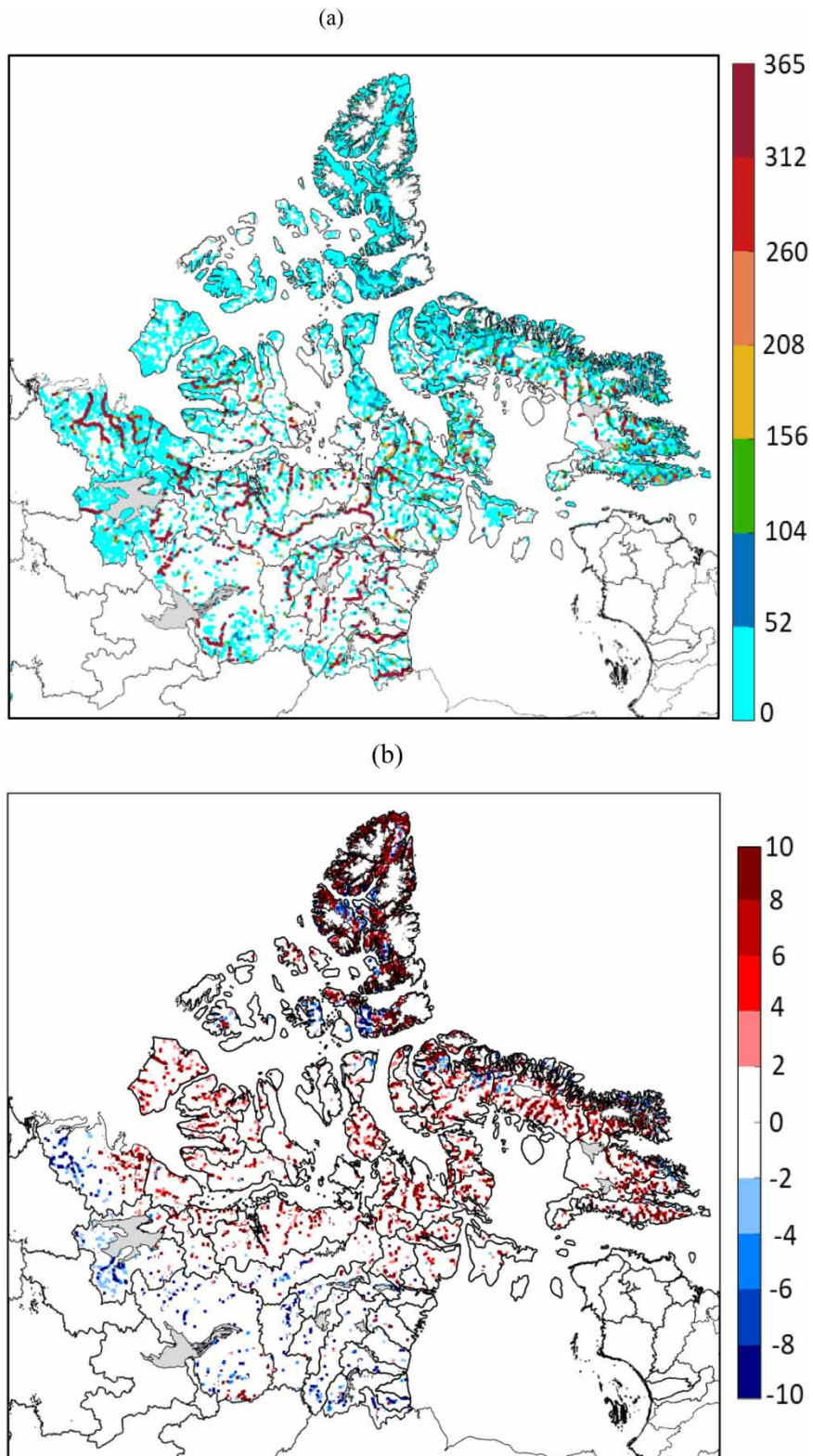


Figure 11 | (a) Annual average number of days with flow velocity greater than 1.5 m/s for the 2001–2020 period (top) and (b) their projected changes for the 2021–2040 period with respect to 2001–2020 period.

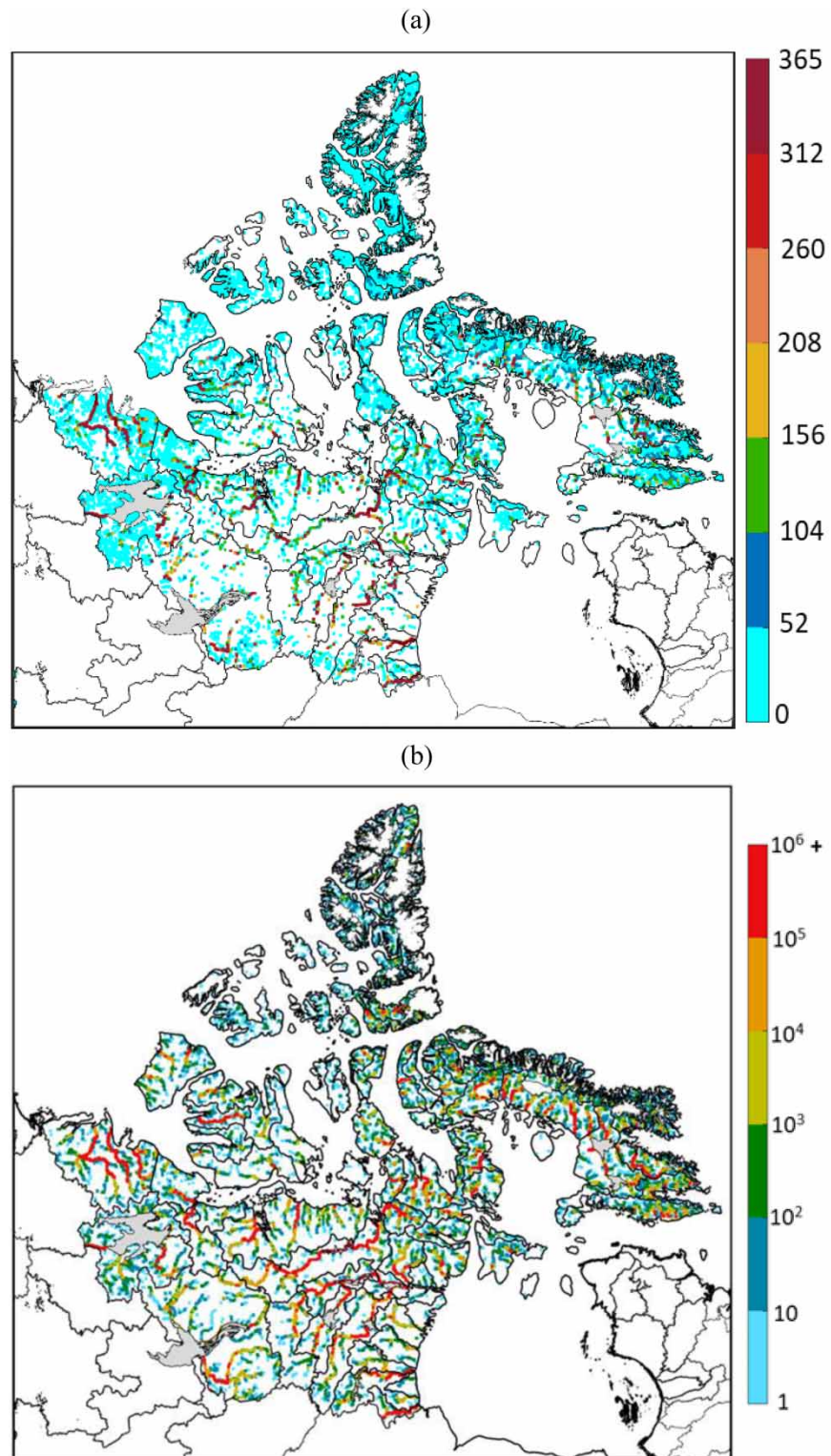


Figure 12 | (a) Annual average number of days with flow velocity greater than 1.5 m/s for the 2001–2020 period with the 30% reduction in flow velocity applied for river ice conditions. (b) Mean annual hydrokinetic power (kW) for the 2001–2020 period with the 30% reduction in flow velocity applied for river ice conditions.

resource-intensive. It is important to note that other cross-sectional shapes may also be utilized depending on specific hydraulic conditions and data availability (Kouwen 2023).

Considering that the extraction of hydrokinetic power can only be realized in future periods, climate warming consequences on the hydrokinetic power potential are also analyzed for the 2021–2040 near-future period for the RCP 8.5 scenario for informed decision-making. It must be noted that this type of analysis for the region is accomplished for the very first time using ultra-high-resolution regional climate model simulations. Although the ability of GEM to simulate various climatic parameters and land features such as soil temperature, air temperature, depth to bedrock, and precipitation characteristics that influence surface runoff and drainage has already been established in the literature (Teufel & Sushama 2022a), some focused evaluations are also accomplished in this study, which seems satisfactory.

The routing scheme considered in this study does not consider the impact of river ice on flow and flow velocity, even though reduced surface runoff in frozen conditions is well captured by GEM. From a hydraulics perspective, the presence of ice cover reduces the water's cross-sectional area and increases the flow resistance, causing reductions in flow velocity and hence flow volume. This altered velocity distribution has important implications for the hydrokinetic power potential of the rivers. There are very few observations of streamflow velocities during river ice conditions. The Water Survey of Canada collected such data during ice-covered conditions for the 1989–1990 winter period at 26 locations across Canada, with most being located in the southern regions of Canada. Hoque (2009), utilizing these observations, quantified the differences in flow velocity between ice-free and ice-covered conditions and reported that the presence of ice cover can reduce streamflow velocities by 30–60%. Applying a reduction of 30% to the velocities obtained in this study during ice cover periods, estimated approximately using a simplified approach as days with 2-m temperature below -2°C in GEM, the number of days with velocity greater than 1.5 m/s decreases in the 0–150 days range, with larger changes noted for the main tributaries over the basins considered (Figure 12(a)) for the current 2001–2020 period. The preliminary investigation, also considering the impact of river ice, confirms the hydrokinetic potential of the basins (Figure 12(b)) discussed in Section 5.

Additional research is needed to better understand streamflow dynamics during ice cover conditions. While ice cover typically increases the flow resistance and reduces surface flow velocity, variations in ice thickness or the formation of ice dams can result in temporary increases in water velocity by elevating the upstream water head (Rokaya *et al.* 2022). Thus, observations of streamflow velocities during river ice conditions are required for the northern regions for in-depth river reach-specific studies, which are very scarce at the moment. This, coupled with hydrodynamic model simulations of flow velocities for river reaches with observed data and machine learning approaches, can contribute to the development of spatio-temporal velocity reduction factors for large-scale applications such as that considered in this study.

7. CONCLUSIONS

From the various analyses and assessments presented and discussed in this paper, the following conclusions can be drawn. Shortcomings of the study and future extensions and research avenues are also highlighted.

1. Comparisons of observed flows from HYDAT with those derived from ERA5 and CanESM2-driven GEM simulations, one way coupled with the WATROUTE scheme, confirm the ability of the climate-hydrology integrated modeling approach in simulating variables that are required for the estimation of hydrokinetic power for the Canadian Arctic River network.
2. Projected changes for the 2021–2040 period with respect to the 2001–2020 period under the RCP 8.5 scenario are minimal for streamflow, flow velocity, and hydrokinetic power over the entire study region. Projected changes could be different in the far future, which is not considered in this study. Increases in the active layer thickness and degrading permafrost conditions in the higher latitudes, projected toward the end of the century, can significantly influence flow patterns and velocities and therefore the hydrokinetic potential of Arctic rivers.
3. As zero-head hydrokinetic turbines can only capture a certain percentage of the kinetic energy of flow, it is important to consider river reaches with flow velocities greater than 1.5 m/s and also where a higher potential of hydrokinetic power exists throughout the year or during a significant part of the year. Further granular analysis of the hydrokinetic power estimates will help in understanding the behavior of individual river reaches and in recommending a suitable hydrokinetic conversion system.
4. The Back (Basin ID: 31) and Back-Hayes (Basin ID: 32) basins along the Arctic coast in central Nunavut and the basins draining into Hudson Bay in the east, which include the Thelon (Basin ID: 5) and Baker Lake (Basin ID: 8) basins, show the highest potential for hydrokinetic power. The Seal (Basin ID 1), Than-anne (Basin ID: 4), and the Thlewaisa (Basin

ID: 2) basins in the southeast of the domain also show potential for hydrokinetic power generation owing to their consistent flow velocity maintained throughout the year.

One of the main limitations of this study is that the projected changes are analyzed based on a single transient climate change GEM simulation for the RCP 8.5 scenario extending until 2040. This was unavoidable and is due to the high computational cost involved in undertaking the ultra-high-resolution simulations at 4 km resolution. To better quantify the uncertainty, it is also useful to consider a multi-model ensemble of simulations at 4 km or even finer resolution. Additionally, the representation of glaciers is considered static and not dynamic, which hinders the accurate representation of streamflow dynamics for glaciated basins. Moreover, due to limited data specific to river channels, the channel modifications due to the installation of turbines, such as the changes in flow velocities and depth of the channel, are not considered in this study. This omission highlights the need for more comprehensive data collection and analysis. Detailed granular studies of the identified reach, employing hydrodynamic models and considering the impact of river ice on the flow volumes and velocities, will contribute to more precise identification of optimal locations and site-specific research for the installation of hydrokinetic conversion systems.

A lack of available information on resource assessments is one of the main limitations in the development of appropriate hydrokinetic energy conversion technology. The ultra-high-resolution climate model coupled with the routing scheme used in the study to estimate flows, flow velocities, and hydrokinetic power for the high-latitude region of Canada contributes toward addressing this deficiency by introducing a science-based approach for hydrokinetic resource assessment and thus reduces reliance on highly uncertain gross regional estimates. This study offers a more reliable assessment, providing valuable and new insights for the development of hydrokinetic energy technologies, and lays the foundation for advanced modeling to support hydrokinetic technology installations.

ACKNOWLEDGEMENTS

This research was funded by the Ocean Coastal and River Engineering Research Center of the National Research Council Canada and the Trottier Institute for Sustainability in Engineering and Design. The simulations considered in this study were performed on the supercomputer managed by Digital Research Alliance and Calcul Québec.

DATA AVAILABILITY STATEMENT

Data cannot be made publicly available; readers should contact the corresponding author for details.

CONFLICT OF INTEREST

The authors declare there is no conflict.

REFERENCES

- Balat, M. (2006) *Hydropower systems and hydropower potential in the European union countries*. *Energy Sources, Part A: Recovery, Utilization and Environmental Effects*, **28** (10), 965–978.
- Bélair, S., Mailhot, J., Girard, C. & Vaillancourt, P. (2005) *Boundary layer and shallow cumulus clouds in a medium-range forecast of a large-scale weather system*, *Monthly Weather Review*, **133** (7), 1938–1960.
- Benoit, R., Côté, J. & Mailhot, J. (1989) *Inclusion of a TKE boundary layer parameterization in the Canadian regional finite-element model*, *Monthly Weather Review*, **117** (8), 1726–1750.
- Clavet-Gaumont, J., Sushama, L., Khaliq, M. N., Huziy, O. & Roy, R. (2013) *Canadian RCM projected changes to high flows for Québec watersheds using regional frequency analysis*, *International Journal of Climatology*, **33** (14), 2940–2955.
- Côté, J., Desmarais, J. G., Gravel, S., Méthot, A., Patoine, A., Roch, M. & Staniforth, A. (1998) *The operational CMC-MRB global environmental multiscale (GEM) model. Part II: results*, *Monthly Weather Review*, **126** (6), 1397–1418.
- David, C. H., Maidment, D. R., Niu, G. Y., Yang, Z. L., Habets, F. & Eijkhout, V. (2011) *River network routing on the NHDPlus dataset*, *Journal of Hydrometeorology*, **12** (5), 913–934.
- Delage, Y. (1997) *Parameterising sub-grid scale vertical transport in atmospheric models under statically stable conditions*, *Boundary-Layer Meteorology*, **82**, 23–48.
- Diro, G. T. & Sushama, L. (2019) *Simulating Canadian Arctic climate at convection-permitting resolution*, *Atmosphere*, **10** (8), 430.
- Döll, P. & Lehner, B. (2002) *Validation of a new global 30-min drainage direction map*, *Journal of Hydrology*, **258** (1–4), 214–231.
- Duvoy, P. & Toniolo, H. (2012) *HYDROKAL: a module for in-stream hydrokinetic resource assessment*, *Computers and Geosciences*, **39**, 171–181.

- Environmental Systems Research Institute (ESRI) (1992) *ArcWorld, 1:3M*, Redlands, CA, USA: ESRI.
- Environmental Systems Research Institute (ESRI) (1993) *Digital Chart of the World, 1:1M*. Redlands, CA, USA: ESRI.
- Gerard, L., Piriou, J. M., Brožková, R., Geleyn, J. F. & Banciu, D. (2009) *Cloud and precipitation parameterization in a meso-gamma-scale operational weather prediction model*, *Monthly Weather Review*, **137** (11), 3960–3977.
- Girard, C., Plante, A., Desgagné, M., McTaggard-Cowan, R., Côté, J., Charron, M., Gravel, S., Lee, V., Patoine, A., Qaddouri, A., Roch, M., Spacek, L., Tanguay, M., Vaillancourt, P. A. & Zadra, A. (2014) Staggered vertical discretization of the Canadian Environmental Multiscale (GEM) model using a coordinate of the log-hydrostatic-pressure type, *Mon. Weather Rev.*, **142**, 1183–1196.
- Guney, M. S. (2011) *Evaluation and measures to increase performance coefficient of hydrokinetic turbines*, *Renewable and Sustainable Energy Reviews*, **15** (8), 3669–3675.
- Hersbach, H., Bell, B., Berrisford, P., Hirahara, S., Horányi, A. & Muñoz-Sabater, J. (2020) *The ERA5 global reanalysis*, *Quarterly Journal of the Royal Meteorological Society*, **146** (730), 1999–2049.
- Hoque, M. A. (2009) *Hydraulic analysis of ice-covered river flow*. Doctoral dissertation. Montreal, QC, Canada: Concordia University.
- Huziy, O., Sushama, L., Khaliq, M. N., Laprise, R., Lehner, B. & Roy, R. (2013) *Analysis of streamflow characteristics over Northeastern Canada in a changing climate*, *Climate Dynamics*, **40** (7–8), 1879–1901.
- Jacobson, P., Ravens, T. M., Cunningham, K. W. & Scott, G. (2012) *Assessment and Mapping of the Riverine Hydrokinetic Resource in the Continental United States*. (No. DOE/EE/0002662-1). Palo Alto, CA, USA: Electric Power Research Institute (EPRI).
- Jia, Y. & Wang, S. S. (2001) *CCHE2D: Two-dimensional hydrodynamic and sediment transport model for unsteady open channel flows over loose bed*. National Center for Computational Hydroscience and Engineering, Technical Report No. NCCHE-TR-2001-1. Oxford, MS, USA: University of Mississippi.
- Johnson, J. B. & Pride, D. J. (2010) *River, tidal, and ocean current hydrokinetic energy technologies: status and future opportunities in Alaska*. Prepared for Alaska Center for Energy and Power., Fairbanks, AK, USA.
- Kain, J. S. & Fritsch, J. M. (1990) *A one-dimensional entraining/detraining plume model and its application in convective parameterization*, *Journal of Atmospheric Sciences*, **47** (23), 2784–2802.
- Khan, M. J., Iqbal, M. T. & Quaicoe, J. E. (2008) *River current energy conversion systems: Progress, prospects and challenges*, *Renewable and Sustainable Energy Reviews*, **12** (8), 2177–2193.
- Khan, M. J., Bhuyan, G., Iqbal, M. T. & Quaicoe, J. E. (2009) *Hydrokinetic energy conversion systems and assessment of horizontal and vertical axis turbines for river and tidal applications: a technology status review*, *Applied Energy*, **86** (10), 1823–1835.
- Khan, Z. U., Ali, Z. & Uddin, E. (2022) *Performance enhancement of vertical axis hydrokinetic turbine using novel blade profile*, *Renewable Energy*, **188**, 801–818.
- Kouwen, N. (2023) *WATFLOOD/CHARM User's Manual*. Waterloo, ON, Canada: University of Waterloo, Environment Canada.
- Kouwen, N., Soulis, E. D., Pietroniro, A., Donald, J. & Harrington, R. A. (1993) *Grouped response units for distributed hydrologic modeling*, *Journal of Water Resources Planning and Management*, **119** (3), 289–305.
- Lee, J. Y., Marotzke, J., Bala, G., Cao, L., Corti, S., Dunne, J. P., Engelbrecht, F., Fischer, E., Fyfe, J. C. & Jones, C. (2021) *IPCC. Climate Change 2021: the Physical Science Basis. In Future Global Climate: Scenario-42 Based Projections and Near-Term Information*, Cambridge, UK: Cambridge University Press.
- Lehner, B. & Döll, P. (2004) *Development and validation of a global database of lakes, reservoirs and wetlands*, *Journal of Hydrology*, **296** (1–4), 1–22.
- Lehner, B., Verdin, K. & Jarvis, A. (2008) *New global hydrography derived from spaceborne elevation data*, *Eos*, **89** (10), 93–94.
- Lehner, B., Verdin, K. & Jarvis, A. (2013) *Technical Documentation Version 1.0*. Sioux Falls, SD, USA: USGS Earth Resources Observation and Science.
- Li, J. & Barker, H. W. (2005) *A radiation algorithm with correlated-k distribution. Part I: local thermal equilibrium*, *Journal of the Atmospheric Sciences*, **62** (2), 286–309.
- Liang, X., Lettenmaier, D. P., Wood, E. F. & Burges, S. J. (1994) *A simple hydrologically based model of land surface water and energy fluxes for general circulation models*, *Journal of Geophysical Research: Atmospheres*, **99** (D7), 14415–14428.
- Milbrandt, J. A. & Yau, M. K. (2005) *A multimoment bulk microphysics parameterization. Part I: analysis of the role of the spectral shape parameter*, *Journal of the Atmospheric Sciences*, **62** (9), 3051–3064.
- Miller, G., Joseph, F., William, L. & Jairo, R. (1986) *The Allocation of Kinetic Hydro Energy Conversion Systems (KHECS) in USA Drainage Basins: Regional Resource and Potential Power*. Final Report, New York, NY, USA: NYUDAS, pp. 86–151.
- Nunavut Water Board (2014) *Nunavut Water Management Areas Descriptions. Appendix B. Nunavut Waters Regulations (SOR/2013-69)*. <https://laws-lois.justice.gc.ca/eng/regulations/SOR-2013-69/FullText.html>.
- Poitras, V., Sushama, L., Seglenieks, F., Khaliq, M. N. & Soulis, E. (2011) *Projected changes to streamflow characteristics over western Canada as simulated by the Canadian RCM*, *Journal of Hydrometeorology*, **12** (6), 1395–1413.
- Prein, A. F., Langhans, W., Fosser, G., Ferrone, A., Ban, N., Goergen, K., Keller, M., Tölle, M., Gutjahr, O., Feser, F. & Brisson, E. (2015) *A review on regional convection-permitting climate modeling: demonstrations, prospects, and challenges*, *Reviews of Geophysics*, **53** (2), 323–361.
- Riahi, K., Rao, S., Krey, V., Cho, C., Chirkov, V., Fischer, G., Kindermann, G., Nakicenovic, N. & Rafaj, P. (2011) *RCP 8.5-A scenario of comparatively high greenhouse gas emissions*, *Climatic Change*, **109** (1), 33–57.

- Ridgill, M., Neill, S. P., Lewis, M. J., Robins, P. E. & Patil, S. D. (2021) Global riverine theoretical hydrokinetic resource assessment, *Renewable Energy*, **174**, 654–665.
- Rokaya, P., Lindenschmidt, K. E., Pietroniro, A. & Clark, M. (2022) Modelling of ice jam floods under past and future climates: a review, *Journal of Hydrology X*, **15**, 100120.
- Saini, G. & Saini, R. P. (2019) A review on technology, configurations, and performance of cross-flow hydrokinetic turbines, *International Journal of Energy Research*, **43** (13), 6639–6679.
- Soulis, E. D., Snelgrove, K. R., Kouwen, N., Seglenieks, F. & Verseghy, D. L. (2000) Towards closing the vertical water balance in Canadian atmospheric models: coupling of the land surface scheme class with the distributed hydrological model watflood, *Atmosphere – Ocean*, **38** (1), 251–269.
- Su, F., Adam, J. C., Bowling, L. C. & Lettenmaier, D. P. (2005) Streamflow simulations of the terrestrial Arctic domain, *Journal of Geophysical Research D: Atmospheres*, **110** (8), 1–25.
- Sushama, L., Laprise, R., Caya, D., Larocque, M. & Slivitzky, M. (2004) On the variable-lag and variable-velocity cell-to-cell routing schemes for climate models, *Atmosphere – Ocean*, **42** (4), 221–233.
- Teufel, B. & Sushama, L. (2019) Abrupt changes across the Arctic permafrost region endanger northern development, *Nature Climate Change*, **9** (11), 858–862.
- Teufel, B. & Sushama, L. (2021) 2°C vs. high warming: transitions to flood-generating mechanisms across Canada. *Water (Switzerland)*, **13** (11), 1494.
- Teufel, B. & Sushama, L. (2022a) High-resolution modelling of climatic hazards relevant for Canada’s northern transportation sector, *Climate Dynamics*, **59** (9–10), 3135–3151.
- Teufel, B. & Sushama, L. (2022b) *Hydrokinetic Resource Assessment for the Canadian Arctic*. Technical Report, Ottawa, ON, Canada: National Research Council Canada, p. 30.
- Teufel, B., Sushama, L., Huziy, O., Diro, G. T., Jeong, D. I., Winger, K., Garnaud, C., de Elia, R., Zwiers, F. W., Matthews, H. D. & Nguyen, V. T. V. (2019) Investigation of the mechanisms leading to the 2017 Montreal flood, *Climate Dynamics*, **52** (7–8), 4193–4206.
- Toniolo, H., Duvoy, P., Vanlesberg, S. & Johnson, J. (2010) Modelling and field measurements in support of the hydrokinetic resource assessment for the Tanana River at Nenana, Alaska, *Proceedings of the Institution of Mechanical Engineers, Part A: Journal of Power and Energy*, **224** (8), 1127–1139.
- Underwood and McLellan, UMA Group (1980) *An Evaluation of the Kinetic Energy of Canadian Rivers & Estuaries*. Technical Report, Ottawa, ON, Canada: Canadian National Research Council-Canadian Hydraulics Centre.
- U. S. Geological Survey (2000) HYDRO1k Elevation Derivative Database. USGS EROS Data Center, Sioux Falls, SD. (Available at <http://edc.usgs.gov/products/elevation/gtopo30/hydro/>).
- Verseghy, D. L. (2011) *CLASS – the Canadian Land Surface Scheme (Version 3.5), Technical Documentation (Version 1)*. Gatineau, QC, USA: Climate Research Division, Science and Technology Branch, Environment Canada.
- WHO (2009) *The Energy Access Situation in Developing Countries*. New York: UNDP WHO. November, 142.
- Woods, J. (2017) *Hydrokinetic Turbine Systems for Remote River Applications in Cold Climates*. Doctoral Dissertation, Winnipeg, MB, Canada: The University of Manitoba.
- Yamazaki, D., Ikeshima, D., Sosa, J., Bates, P. D., Allen, G. H. & Pavelsky, T. M. (2019) MERIT hydro: a high-Resolution global hydrography Map based on latest topography dataset, *Water Resources Research*, **55** (6), 5053–5073.
- Zhang, S., Gan, T. Y., Bush, A. B. G. & Zhang, G. (2023) Evaluation of the impact of climate change on the streamflow of major pan-Arctic river basins through machine learning models, *Journal of Hydrology*, **619**, 129295.
- Zhang, Y. (2018) *CCHE-GUI – Graphical Users Interface for NCCHE Models User’s Manual*. NCCHE-TR-2013-01. Oxford, MS, USA: National Center for Computational Hydroscience and Engineering (NCCHE).

First received 24 April 2024; accepted in revised form 4 March 2025. Available online 12 March 2025